Open Ceramics 14 (2023) 100365

Contents lists available at ScienceDirect

Open Ceramics

journal homepage: www.sciencedirect.com/journal/open-ceramics

A new brick-type using grape stalks waste from wine production as pore-agent

Chiara Coletti [a,*], Emily Bragié [a,b], Maria Chiara Dalconi [a], Claudio Mazzoli [a], Anno Hein [c], Lara Maritan [a]

[a] Department of Geosciences, University of Padova, Via G. Gradenigo 6, 35131, Padova, Italy
[b] C.S.G. Palladio S.r.l., Strada di Saviabona, 278/1A, 36100, Vicenza, Italy
[c] Institute of Nanoscience and Nanotechnology, N.C.S.R. 'Demokritos', Aghia Paraskevi, 15310, Athens, Greece

ARTICLE INFO

Handling Editor: Dr P Colombo

ABSTRACT

Under the motivation of the Agenda 2030, increasing efforts have been addressed to the introduction of green products into the marketplace, enhancing awareness on eco-labelling and supporting the industrial sustainable development. This study investigates the re-use of waste generated by wine production (10 vol % of milled grape stalks were added to a standard clay body) as a new primary resource in making high porous bricks. Results demonstrate that the combustion of grape stalks during the firing process gives several advantages, in particular related to the formation of macro-pores (up to 4 cm). Large pores, in fact, make this experimental new brick-type a high-quality material both in terms of insulating performances, drastically reducing the heat transmission, and of resistance in environmental stressed conditions, specifically where salts or temperatures around 0 °C (for cycles of ice formation) can occur.

1. Introduction

1.1. New material design challenge and the agenda 2030

Nowadays is well known that a society exclusively relying on linear economy is an historical anomaly in terms of resource exploitation. The culture of reuse in ceramic industry is rooted in the past [1–6] and represents an alternative for win-win circular economy solutions, still able to face modern industrial challenges in a sustainable perspective. On this lesson from the past, the UN General Assembly agreed on the Sustainable Development Goals (SDGs) of the Agenda 2030 (United Nation-UN, 2015), according to which a sustainable development emphasizes the enhancement of environmental, social and economic resources, in order to meet the needs of current and future generations. Since the building materials industry has a strong impact on the environmental issues, it can widely contribute to achieving the UN SDGs goals [7]. One of the challenges to face is a more sustainable use of natural resources, as reported at the EU level by the Raw Material Initiative [8], considering also the entire life cycle (LCA, Life Cycle Assessment) of the product. Under these perspectives, all phases of the chain of production and their impacts are assessed, including processes for extraction and processing of raw materials, transport and distribution, use and/or re-use of waste and by-products, storage, and end material management [9].

1.2. State-of-the-art

Numerous studies have been carried out over the last three decades on the re-use of waste and by-products as a successful resource in the production of new bricks, such as those tested by incorporating organic materials [10–17], or those addressed to the addition of inorganic waste derived for instance from natural stone processing [15,18–24], and industrial sludges [25–27]. Nevertheless, although results achieved were often very promising, the implementation of commercial bricks with recycled waste materials in the industrial sector is still limited (Table 1).

Concerning the use of organic-type additive (such as plants, grass, rise, wood-ash, shells, born or hair) into the clay paste is attested since the prehistoric time [28–32] and it is frequently used also as pore-forming agent in previous literature for new mix designs [10–12, 33,34].

* Corresponding author.
E-mail address: chiara.coletti@unipd.it (C. Coletti).

https://doi.org/10.1016/j.oceram.2023.100365
Received 28 March 2023; Accepted 27 April 2023
Available online 4 May 2023

Table 1
State-of-the-art (SoA), gaps and how these gaps can be addressed.

Area	SoA	Gap	How to address the gap
Industrial implementation of commercial bricks with recycled waste	Very promising results from previous researches	Sporadic partnerships between academic research and industry in this technological area	Active collaborations between academic and industrial worlds
		Absence of standard procedures fulfilling requirements for the evaluation of processes and finished products	Applying standard procedures in order to define guideline to quantify the impact on economic and environmental issues
		Widespread public skepticism due to poor public education on the possible sustainable frontiers	Allowing conscious eco-labelling and adequate public education about the high potential of these materials, also recovering awareness in ancient habit of reuse from the past

1.3. The main scope of the study

In this work, discards from wine production (grape stalks) were used as secondary resource to produce a new highly-porous brick type.

The large quantity of residual grapes from the wine activity is processed to obtain ashes or commonly dumped in landfills for animal feed [35,36]. This procedure leads to higher cost and may damage the soil, contributing to air pollution for methane and carbon dioxide emissions released by decomposition and anaerobic degradation of organic material, which can be potential source for the greenhouse gases (GHG). Although grape stalks are not intrinsically hazardous, the fact that production is concentrated in a period of the year poses potential pollution issues and implications for global warming and climate change. In addition, space limitations of the disposal in landfills can also give other problematic circumstances, due to smells and noises. For all these reasons wine producers are really interested to find new solutions for these discards/wastes, especially in terms of their re-use in a sustainable way.

On the basis to these needs, the present study addresses the following specific objectives: i) to assess the pore system and micro-structures providing hints for the optimization of brick quality; ii) to verify the final physical properties (e.g. water behaviour and thermal insulation); iii) to evaluate the durability in presence of ice and salts growth in relation to the pore structure before and after ageing tests.

This research supports the development of the circular economy according to the LCA principles, thus, using local resources and producing lightweight bricks, saving energy and costs in transport.

2. Materials and methods

In this work two brick types (samples B1 and B2, Table 2) were obtained using a clay material (*Rosso Casaglia Forte,* the complete chemical and mineralogical characterization of which is reported in Coletti et al., 2018 [19]) chemically rich in SiO_2 (57.77 wt %) and Al_2O_3 (14.14 wt %) as it was (Brick B1) and adding to it (Brick B2) 10 % (vol.) of dry grapes milled up to 2 mm-size. Both samples were obtained by means of a soft-mud moulding process and fired 950 °C.

Table 2
Description of the analysed samples.

Sample	Additive type	vol. % of additive	Firing Temperature (°C)
B1	–	–	950 °C
B2	grape stalks	10 (vol %)	

Table 3
Analytical approach. Scope and type of analyses performed and instrumental conditions or procedures adopted.

Scope	Analysis	Conditions/Parameters used
Mineralogy	X-Ray Powder Diffraction (XRPD)	PANalytical X'Pert PRO diffractometer, operating in Bragg-Brentano reflection geometry with CoKα radiation, 40 kV of voltage and 40 mA of filament current, equipped with an X'Celerator detector. Semi-quantitative analysis was obtained by applying the Rietveld method (Topas v4.1 software) [37] adding 10 wt % of the internal standard zincite (J.T. Baker).
Porosity	Digital Imaging Analysis (DIA) from Scanning Electron Microscopy Backscattered electron (SEM-BSE) images	SEM-BSE images (1280 × 1024 pixel) were acquired with a CamScan MX 2500 microscope, equipped with a LaB_6 cathode, operating at 20 kV, working distance (WD). The analyses were performed on a stitching of 900 images at 200 × magnification on thin sections of dimensions 3×2.5 cm^2 and of 1200 images at 50 × magnification 4.5 × 3 cm^2. All the images produced are processed with the ImageJ® software [38]. Threshold limits: 2 μm for images acquired at 200×; 0.5 μm for those acquired at 50×.
Water behaviour	Hydric test (HT)	Water Absorption was tested on cubic samples (50 mm edge) (three samples per type of brick) [39]. Free and forced absorption (Al and Af), apparent and skeletal density (d_a and d_r), open porosity (P) and degree of pore interconnection (Ax) were calculated.
	Capillarity	Capillary coefficient (Ks) and rise (B) were studied on three prism-shaped samples (25 × 25 × 120 mm) for each brick type [40].
Thermal conductivity	InfraRed (IR) Thermocamera	Thermal diffusion was studied using an InfraRed-Thermocamera (FLIR) by heating cubic samples (edge: 50 mm) to 50 °C (with a heating plate) for 20 min. IR-images were captured in time lapse mode every 30 s [41]. The IR-images and the profiles of thermal diffusion were extrapolated after 6 min of heating.
	Thermal analyser	Thermal conductivity of disk-shaped samples (thickness: 5 mm, diameter: 30 mm) was determined with a steady-state hot-disk set-up [19,42,43]. Measurements were taken at three heat source temperatures: 100, 200 and 300 °C.
Durability (aging tests)	Freeze-thaw test	Frost resistance was evaluated by the freeze–thaw test on three cubic samples (edge: 50 mm) for each brick type through 30 cycles of 24 h [44]. Weight loss (ΔM/M) was calculated on samples after each cycle.
	Salt crystallization test	Resistance to salt crystallization was determined on three cubic samples (edge: 50 mm) for each brick type subjected to 10 cycles of 24 h each [45]. Weight loss (ΔM/M) was calculated on samples after each cycle.

Table 4
Mineralogical assemblages of the fired bricks (samples B1 and B2). Semi-quantitative analysis (%) calculated by Rietveld method. Minerals abbreviation according to Warr (2021) [46]: Qz = quartz; Pl = plagioclase; Sa = sanidine; Di = diopside; Hem = hematite; Gh = gehlenite. AM = amorphous phase.

Samples	Qz	Pl	Sa	Di	Hem	Gh	AM
B1	29.0	27.6	7.7	3.5	1.6	2.4	17.0
B2	27.6	26.5	6.7	3.1	2.2	1.2	22.0

The two bricks, the one obtained by the reference clay and the other one being the new mix design, were compared, adopting a multidisciplinary approach at different scale (from micro- to macro-scale) to test the brick features. For this purpose, mineralogy of samples (B1 and B2) and their physical properties, such as porosity, water behaviour, thermal conductivity and durability, were measured (Table 3) and compared.

3. Results and discussion

3.1. Mineralogy

Samples B1 and B2 are very similar in mineralogical composition and abundance (Table 4). Both bricks, indeed, display a major content of quartz (29.0 % and 27.6 % for samples B1 and B2, respectively), followed by plagioclase (27.6 and 26.5 %). New silicate phases derived by the pyrometamorphic process (transformation related to the increase of temperature during firing) are also present: diopside, gehlenite, and hematite [47–49]. Sanidine (high-temperature polymorph of K-feldspar), observed in the diffraction patterns, around 7.0 % in both samples, can have a twofold origin, as relic minerals of clay [18], or as new

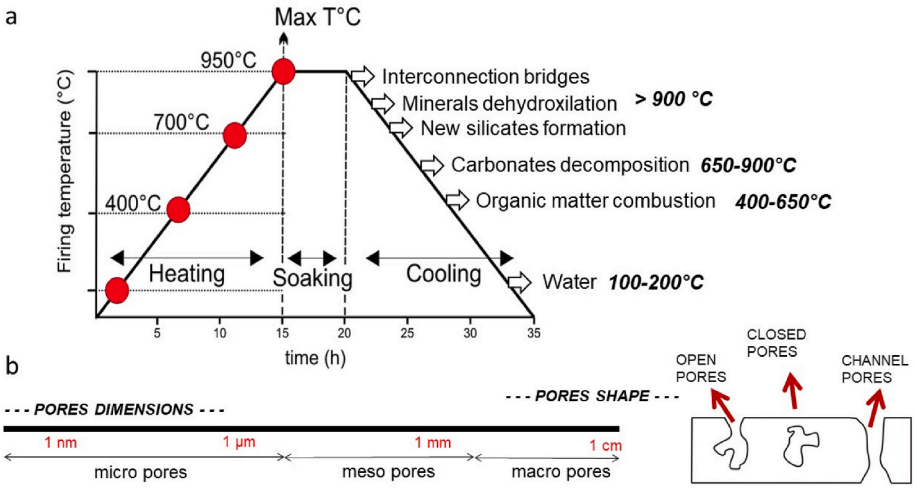

Fig. 1. a) Schematic representation of the main steps of mineralogical and textural evolution during firing of brick-types with organic materials (maximum temperature reached 950 °C). b) Synthetic classification of pores for dimensions [19,52] and type.

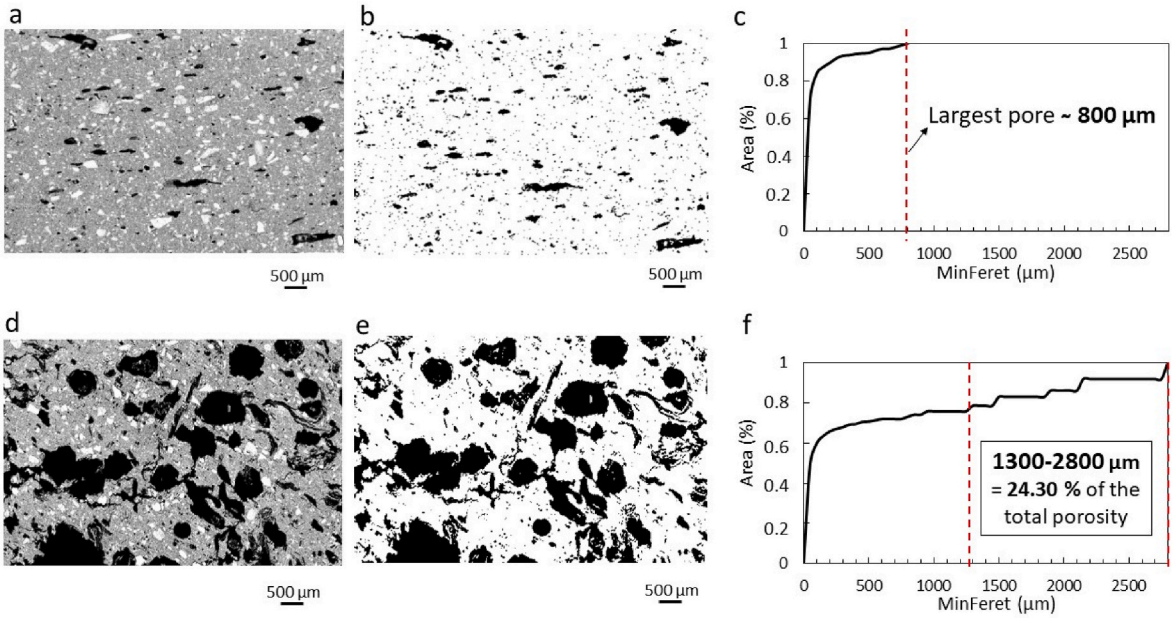

Fig. 2. Results form the DIA of SEM-BSE grey-scale images: a) SEM-BSE of sample B1 obtained stitching together 900 overlapping images taken at a magnification of 200× (total area of the stitched image ~ 5 cm^2); b) binary image of sample B1 (pores in black) obtained from SEM-BSE image (a); c) Cumulative porosimetric curve of sample B1 obtained by DIA (b); d) SEM-BSE of sample B2 obtained stitching together 900 overlapping images taken at a magnification of 200× (total area of the stitched image ~ 5 cm^2); e) binary image of sample B2 (pores in black) obtained from SEM-BSE image (d); f) Cumulative porosimetric curve of sample B2 obtained by DIA (e).

Table 5
Physical properties of the fired bricks (samples B1 and B2). DIA 50×: na_{50} = Total porosity (%) by DIA at 50× of magnification; 5–100 = % of na_{50}, detected in pore range 5–100 μm by DIA; 200–500 = % of na_{50}, detected in pore range 200–500 μm by DIA; >500 = % of na_{50}, detected in pore range >500 μm by DIA; 1300–2800 = % of na_{50}, detected in pore range 1300–2800 μm by DIA. DIA 200x: na_{200} = Total porosity (%) by DIA at 200× of magnification; >1000 = % of na_{200}, detected in pore range >500 μm by DIA; MinFeret = maximum pore diameter measured at 200x. Water Absorption (HT) & Capillarity: P = total porosity (%) calculated by HT; Al = % of free water absorbed; Af = % of forced water absorbed; Ax = pore interconnection; d_a = apparent density (g/cm^3); d_r = rea density (g/cm^3); Ks = coefficient of capillarity; B = capillary rise. Thermal conductivity: λ = thermal conductivity (W/(m·k)) measured at 100 °C, 200 °C and 300 °C.

	DIA 50×					Water Absorption (HT) & Capillarity							
Sample	na_{50}	5–100	200–500	>500	1300–2800	P	Al	Af	Ax	d_a	d_r	Ks	B
B1	19.80	84.00	7.00	4.00	–	36.22	21.62	22.12	2.26	1.64	2.57	0.40	1.20
B2	26.20	59.70	7.40	29.30	24.30	58.63	39.42	47.64	17.26	1.23	3.00	1.50	3.10

	DIA 200x			Thermal conductivity		
Sample	na_{200}	>1000	MinFeret	100 (°C)	200 (°C)	300 (°C)
$B1_X$	–	–	–	0.96	0.89	0.90
$B1_{Y/Z}$	–	–	–	0.91	0.84	0.80
$B2_X$	22.80	52.09	6500	0.64	0.60	0.60
$B2_Y$	26.10	61.97	9600	0.58	0.59	0.59
$B2_Z$	26.30	66.82	13900	0.55	0.57	0.58

formed mineral during firing (> 800 °C) [50,51]. The amorphous content (AM, Table 4) is the main difference evidenced by Rietveld semi-quantitative analysis being estimated at 17.0 % for sample B1 and at 22.0 % for sample B2. The highsintering in the sample B2 can be explained by the enhance of temperature during organic combustion (more or less at 600 °C) which occurs with a strong exothermic reaction, increasing melting along grape stalk sites when pores developed (see supplementary materials, Fig. 1S).

3.2. Physical properties

3.2.1. Porosity

DIA allowed to characterize the porosity of the samples and to evaluate differences in terms of pore abundance, grain-size distribution and shape.

Sample B1 (Fig. 2a and b) has a total porosity of 19.80 %, where most of the pores (84 % of the total porosity) are comprised in the range 5–100 μm, 7 % between 200 and 500 μm, and just 4 % felt over 500 μm with the largest pore around 800 μm (Table 5, Fig. 2c). Sample B2 (Fig. 2d and e) displays a total porosity of 26.20 %, in which 59.70 % of it is comprises between 5 and 100 μm, while meso-pores with dimensions above 500 μm are very abundant. Indeed, 29.30 % of pores (of the total porosity) falls in this latter range, 24.30 % of which are macro-pores with millimetric dimensions (1300–2800 μm) (Table 5, Fig. 2f).

Although both samples were fired at 950 °C, and new pores formed after paste and absorbed water evaporation, minerals dihydroxylation, and calcite decarbonation, sample B2 has a final porosity much higher than that estimated in sample B1 by the effect of the organic-additive combustion occurring up to 600 °C (Fig. 1 and see videos in supplementary materials, Fig. 1Sa,b). Indeed, the grape stalks waste acts as pore-agent and its combustion left large pores, with dimensions up to some millimetres (2800 μm; Table 5).

Since the large size of pores, sample B2 was analysed (at 50× of magnification) also on a larger area (thin sections 4.5 × 3 cm^2), thus to optimise the results in terms of representativeness [37]. That allowed to also observed that, being most of pores formed by grape stalks combustions, they have elongated shapes along the three orthogonal directions. Indeed, sample B2 analysed by DIA on thin sections obtained by the three orthogonal directions ($B2_X$, $B2_Y$ and $B2_Z$; Fig. 2c, Table 5) shows different arrangements and abundances of pores. Results

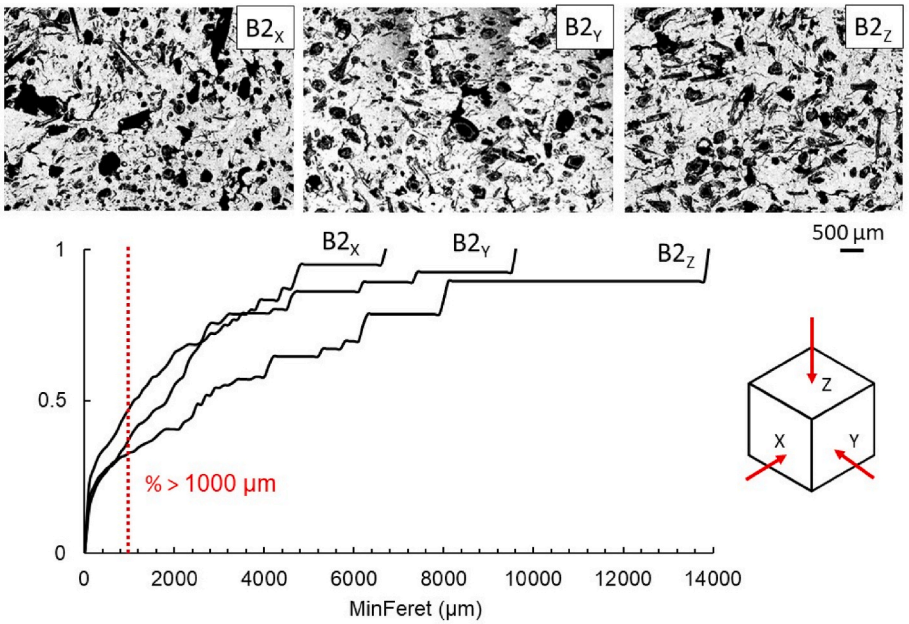

Fig. 3. Porosimetric curves obtained by DIA along the three different orientations ($B2_X$, $B2_Y$ and $B2_Z$) of brick B2. Results obtained stitching together 1200 overlapping images at a magnification of 50×, total area of the stitched image ~8 cm^2, as reported on the top of the figure.

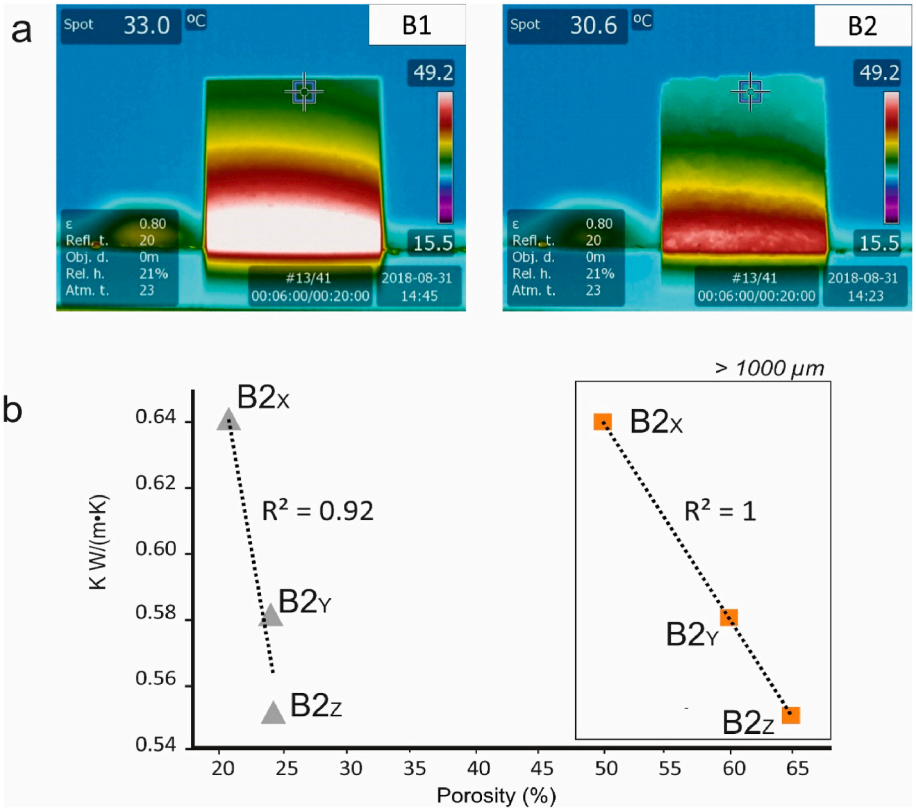

Fig. 4. Thermal conducitivity: a) qualitative analysis by means IR-images: comparison between images in false colors of samples B1 and B2 after 6 min of heating (at 50 °C); b) Graph reporting quantitative results obtained by thermal analysis with the steady-state hot-disk set-up measured at 100 °C (λ = W/(m·k); y axis) along three othogonal direction (X, Y and Z) measured on sample B2 and the respective porosity calculated (%) by DIA (na_{200} = %; x axis). The grey triangles in the left are the λ correlated to the total porosity by DIA (na_{200}). On the right, in the square, the same the λ correlated to the porosity calculated by DIA (at 200x) above 1000 µm (Table 5). (For interpretation of the references to color in this figure legend, the reader is referred to the Web version of this article.)

demonstrated that: i) the side $B2_X$ displays 22.80 % of pores (52.09 % of them > 1000 µm), with the maximum size at more than 6 mm (6500 µm); ii) the side $B2_Y$ has a porosity of 26.10 % (61.97 % of them > 1000 µm) with the largest pore almost centimetric (the maximum MinFeret was measured at 9600 µm); and iii) the side $B2_Z$ has a total porosity of 26.30% (66.82 % of them > 1000 µm) with the largest pore measured at 13900 µm (Fig. 3). These results confirmed the high structural anisotropy due to the brick manufacturing (forming for pressing in moulds) that orients grape stalks perpendicular to the pressure direction ($B2_Z$) and consequently the pores during combustion. Where grape stalks collapse, pores formed on their original shape (Fig. 1Sb).

3.2.2. Water behaviour

Total porosity calculated by HT confirmed results obtained by DIA, although with a higher pore abundance in both samples: 36.22 and 58.63 % for sample B1 and B2, respectively (Table 5). This discrepancy can be attributed to different methods used. Indeed, DIA is useful for extrapolating information about pore size and shape, totally disregarded by HT, although it can have some instrumental limitations mainly due to the threshold limit defined by SEM-BSE images resolution [37]. According to our operational conditions, all pores below the threshold limit of 0.5 µm, for DIA reconstruction at 200× of magnification, and of 5 µm, at 200× of magnification, are not observed.

Sample B2 showed higher water absorption compared to sample B1 (Al = 39.42, Af = 47.64 %), but is the sample with the worst pore connection system (Ax = 17.26 for sample B2, against the Ax = 2.26 of sample B1) (Table 5). It suggests that the latter is characterized by a more complex pore system [49] with in which there are pores with small access, which hinders water movement inside the brick.

As expected, apparent density is lower for sample B2 which has a value of d_a = 1.23 g/cm^3, while sample B1 has a value of d_a = 1.60 g/cm^3. The trend is different for the real densities. Indeed, bricks obtained with the addition of grape stalks have a real density higher (3.00 g/cm^3) than that calculated for the sample B1 (2.57 g/cm^3) (Table 5). This increased intrinsic density confirms the more advanced sintering process during firing due to the organic phase combustion, as noted in the amorphous content by XRPD analysis (Table 4).

Sample B2 is the most susceptible to capillarity rise (Ks = 1.50), whereas sample B1 has a lower Ks value (Ks = 0.40) (Table 5). Capillarity shows as for HT a higher aptitude to absorb water of sample B2. Both the coefficient of capillarity and the capillary rise values (Ks and B, respectively) are higher for this sample (Ks = 1.50; B = 3.10). Being this behaviour related to the presence of capillarity pores (0.1–10 µm) [38, 53], it suggests a certain abundance of pores in this range, not detected by DIA.

3.2.3. Thermal conductivity

Thermal conductivity was measured qualitatevely by IR acquisitions and quantitatevely by a thermal analyser.

IR-images clearly reveal the different behaviour of the two studied samples in heat transmission (see videos in Supplementary Materials, Fig. 2Sa and 2Sb). The most compact brick (sample B1) after 6 min from the beginning of the test (Fig. 3a) shows an high white band (up to the half of the cubic sample) which corresponds to the part of the sample in which temperature reached 50 °C (the same temperaure of the heating plate). Otherwise, at the same time (after 6 min) heat is trasmissed slower in sample B2, which does not display the reaching temperature of 50 °C neither in the contact surface with the plate. The spot of measure on the top of the samples (50 × 50 × 50 mm) points out a difference of a 2.4 °C according to the temperature reached by the two bricks: 33.0 °C and 30.6 °C for brick B1 and B2, respectively (Fig. 4a).

The insulating behaviour of sample B2 was also verified by measurements with the steady-state hot-disk set-up thermal analyser. Sample B1, measured on two perpendicalur directions ($B1_X$ and $B1_{Y/Z}$), has λ values > 0.90 W/(m·k), while brick B2 always has λ values < 0.70 W/(m·k) in all the three direction measured ($B2_X$, $B2_Y$ and $B2_Z$) (Table 5). These results are in agreement with the pores abundance of the two samples (detected by DIA and HT, Table 5), as reported by Allegretta

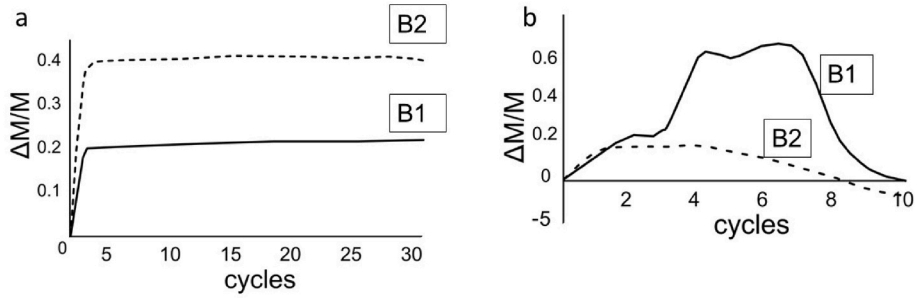

Fig. 5. Durability (ageing tests): a) weight variation (ΔM/M) during 30 freeze-thaw cycles on bricks; b) weight variation (ΔM/M) during 10 salt crystallization cycles on bricks.

et al., 2017 [42] (Fig. 4b). If in brick B1 thermal conductivity shows a slight difference along the X and the Y/Z axes ($B1_X$, $B1_{Y/Z}$), in the brick B2 results stressed a strong thermal anisotropy along the three orientations, in particular when the analyser heats samples at 100 °C (Table 5). This agrees with the porosity estimated by DIA (Table 5, DIA 200x), as a consequence of the orientation of grape stalks in the brick during its moulding.

Correlation between pores abundance and their capacity to reduce the heat transmission is particularly closed if we consider the largest pores. It is well explained by plotting the thermal conductivity (λ measured at 100 °C) along the three directions of the brick B2 and the percentage of pores (% of total porosity, DIA 200x, > 1000, Table 5) with dimensions above 1000 μm ($R^2 = 1$; Fig. 4b).

3.3. Durability

Both brick types display a good durability during salt crystallization and freeze–thaw cycles. Damage after the ageing tests was confined mainly to the edges and vertices of the cubic samples, with poor loss of material. Weight loss after freeze–thaw cycles, indeed, is recorded at 1 wt % for brick B2 and 0 wt % for sample B1, corresponding to 1.5 and 0 g, respectively. In the case of salt crystallization, the weight change after testing is of 5 wt % for brick B1 (11.42 g) and 3 wt % for sample B2 (5.60 g). Considering the weight variation curves, after the immersion in the solution during the freeze-thaw test, sample B2 shows an immediate weight increase, due to its high-water absorption (Table 5), and no relevant weight variation (Fig. 5a). A similar trend is displayed for sample B1. Different behaviour during the test is recorder for samples subjected to the salt crystallization test (Fig. 5b). In this case, sample B1 increases its weight during the ageing test due to the salts growth within pores, which then release in solution during the last cycles. While, sample B2 trapped less salts, probably due to its large pores.

4. Conclusions

This study investigated the possibility to introduce grape stalks for minimizing environmental impact derived from the wine activity and for generating new value-added brick.

Results demonstrated that grapes stalk combustion increases the porosity of the final product both in terms of abundance (total porosity, %) and of pore dimensions, enhancing durability and thermal insulation properties. Large size of pores (up to 3–4 cm), indeed, favors a good durability, reducing the pressure effects due to ice and salt crystallization during freeze-thaw and salt solution cycles. The high abundance of pores and their elongated shapes due to the grape stalks' combustion decreases the heat transmission of around 40 % with respect to the same type of clay. These characteristics assess the possible implementation of grapes stalk as pore agent in new mix designs. Due to the high porosity (~ 58 % by HT), it cannot be used as building materials, since lacks an adequate load capacity, but it can be implemented in the market for insulting covering in houses both in indoor and outdoor conditions.

The development of the high-quality bricks with enhanced thermal properties means saving energy for heating houses, and thus saving first the environment and then the economic costs; moreover, the high porosity of the final product (obtaining a lightweight brick) and the local provision of the material has a twofold direct LCA impact during material transport.

Declaration of competing interest

The authors declare that they have no known competing financial interests or personal relationships that could have appeared to influence the work reported in this paper.

Acknowledgments

The authors thank the *SanmarcoTerreal srl* for supporting research with the brick production and the wine cellar *La Cantina di Conegliano e Vittorio Veneto sac* for providing the grape stalks.

Appendix A. Supplementary data

Supplementary data to this article can be found online at https://doi.org/10.1016/j.oceram.2023.100365.

References

[1] L. Maritan, C. Mazzoli, M. Tenconi, G. Leonardi, S. Boaro, Provenance and production technology of early bronze age pottery from a lake dwelling settlement at Arquà Petrarca (Padova, NE Italy), in: P.S. Quinn (Ed.), Interpreting Silent Artefacts: Petrographic Approaches to Archaeological Ceramics, Archaeopress, Oxford, 2009, pp. 81–99, 2009.

[2] M. Tenconi, L. Maritan, G. Leonardi, B. Prosdocimi, C. Mazzoli, Ceramic production and distribution in North-East Italy: study of a possible trade network between Friuli Venezia Giulia and Veneto regions during the final Bronze Age and early Iron Age through analysis of peculiar "flared rim and flat lip" pottery, Appl. Clay Sci. 82 (2013) 121–134.

[3] G. Eramo, A. Aprile, I.M. Muntoni, A. Zerboni, Textural and morphometric analysis applied to holocene pottery from takarkori rock shelter (SW Libya, central sahara): a quantitative sedimentological approach, Archaeometry 56 (2014) 36–57.

[4] E. Holmqvist, M. Larsson, A. Kriiska, V. Palonen, P. Pesonen, K. Mizohata, P. Kouki, L. Räisänen, Tracing grog and pots to reveal neolithic corded ware culture contacts in the baltic sea region (SEM-EDS, PIXE), J. Archaeol. Sci. 91 (2018) 77–91.

[5] G. Eramo, Ceramic technology: how to recognize clay processing, Archaeol. Anthropol. Sci. 12 (2020) 164, https://doi.org/10.1007/s12520-020-01132-z.

[6] L. Maritan, G. Ganzarolli, F. Antonelli, M. Rigo, A. Kapatza, K. Bajnok, C. Coletti, C. Mazzoli, L. Lazzarini, P. Vedovetto, A. Chavarría Arnau, What kind of calcite? Disclosing the origin of sparry calcite temper in ancient ceramics, J. Archaeol. Sci. 129 (2021), 105358, https://doi.org/10.1016/j.jas.2021.105358.

[7] M.A.B. Omer, T. Noguchi, A conceptual framework for understanding the contribution of building materials in the achievement of Sustainable Development Goals (SDGs), Sustain. Cities Soc. 52 (2021), 101869, https://doi.org/10.1016/j.scs.2019.101869.

[8] Policy and strategy for raw materials internal market, industry, entrepreneurship and SMEs, Available online: https://ec.europa.eu/growth/sectors/raw-materials/policy-strategy_en. (Accessed 28 December 2020).

[9] ISO—ISO 14040, Environmental management—life cycle assessment, Principles and Framework, ISO/TC 207/SC 5, Life cycle assessment (2006). Edition 2, 20 pages. Available online: https://www.iso.org/standard/37456.html. (Accessed 29 December 2020).

[10] I. Demir, An investigation on the production of construction brick with processed waste tea, Build. Environ. 41 (2006) 1274–1278.
[11] I. Demir, Effect of organic residues addition on the technological properties of clay bricks, J. Waste Manag. 28 (3) (2008) 622–627.
[12] D. Eliche-Quesada, M.A. Felipe-Sesé, J.A. López-Pérez, A. Infantes-Molina, Characterization and evaluation of rice husk ash and wood ash in sustainable clay matrix bricks, Ceram. Int. 43 (2016) 463–475.
[13] L. Barbieri, Lancellotti I. Andreola, R. Taurino, Management of agricultural biomass wastes: preliminary study on characterization and valorisation in clay matrix bricks, Waste Manag. 33 (2013) 2307–2315, https://doi.org/10.1016/j.wasman.2013.03.014.
[14] L. Aouba, C. Bories, M. Coutand, B. Perrin, H. Lemercier, Properties of fired clay bricks with incorporated biomasses: cases of olive stone flour and wheat straw residues, Construct. Build. Mater. 102 (1) (2016), https://doi.org/10.1016/j.conbuildmat.2015.10.040, 7–13.
[15] S.M.S. Kazmi, m. Junaid Munir, Y.-F. Wu, a. Hanif, I. Patnaikuni, Thermal performance evaluation of eco-friendly bricks incorporating waste glass sludge, J. Clean. Prod. 172 (2018) 1867–1880, https://doi.org/10.1016/j.jclepro.2017.11.255.
[16] O. Kizinievič, V. Kizinievič, I. Pundiene, D. Molotokas, Eco-friendly fired clay brick manufactured with agricultural solid waste, Arch. Civ. Mech. Eng. 18 (Issue 4) (2018) 1156–1165, https://doi.org/10.1016/j.acme.2018.03.003.
[17] N. Cobîrzan, G. Thalmaier, A.A. Balog, H. Constantinescu, I. Timiș, M. Streza, Thermophysical properties of fired clay bricks with waste ceramics and paper pulp as pore-forming agent, J. Therm. Anal. Calorim. 134 (2018) 843–851, https://doi.org/10.1007/s10973-018-7092-3.
[18] M. Sütçü, H. Alptekin, E. Erdogmus, Y. Er, O. Gencel, Characteristics of fired clay bricks with waste marble powder addition as building materials, Construct. Build. Mater. 82 (2015) 1–8, https://doi.org/10.1016/j.conbuildmat.2015.02.055.
[19] C. Coletti, L. Maritan, G. Cultrone, A. Hein, M.C. Dalconi, E. Molina, C. Mazzoli, Recycling trachyte waste from quarry to brick industry: effects on petrophysical properties and durability of new bricks, Construct. Build. Mater. 166 (2018) 792–807, https://doi.org/10.1016/j.conbuildmat.2018.01.158.
[20] S. Kang, S. Yoo, J. Lee, B. Boo, H. Ryu, Experimental investigations for recycling of silicon and glass from waste photovoltaic modules, Renew. Energy 47 (C) (2012) 152–159.
[21] V.M. Fthenakis, End-of-life management and recycling of PV modules, Energy Pol. 28 (2000) 1051.
[22] N. Phonpuok, S. Kanyakam, P. Chindaprasirt, Utilization of waste glass to enhance physical–mechanical properties of fired clay brick, J. Clean. Prod. 112 (2016) 3058–3062.
[23] J.M. Inocente, V.S. Nandi, F. Rosso, A. de Oliveira, A. Zaccaron, Study for vitreous waste recovery in the formulation of heavy clay ceramics, Material Sci & Eng Int J. 1 (2) (2017) 56–60, https://doi.org/10.15406/mseij.2017.01.00010.
[24] L. Crespo-López López, G. Cultrone, Improvement in the petrophysical properties of solid bricks by adding household glass waste, J. Build. Eng. 59 (1) (2022), 105039, https://doi.org/10.1016/j.jobe.2022.105039.
[25] C. Coletti, L. Maritan, G. Cultrone, C. Mazzoli, Use of industrial ceramic sludge in brick production: effect on aesthetic quality and physical properties, Construct. Build. Mater. 124 (2016) 219–227, https://doi.org/10.1016/j.conbuildmat.2016.07.096.
[26] G. Cultrone, E. Sebastián, Fly ash addition in clayey materials to improve the quality of solid bricks, Construct. Build. Mater. 23 (2009) 1178–1184.
[27] E. Erdogmus, M. Harja, O. Gencel, M. Sütçü, A. Yaras, New construction materials synthesized from water treatment sludge and fired clay brick wastes, J. Build. Eng. 42 (2021), 102471, https://doi.org/10.1016/j.jobe.2021.102471.
[28] J.M. Skibo, M.B. Schiffer, K.C. Reid, Organic-tempered pottery: an experimental study, Am. Antiq. 54 (1989) 122–146.
[29] O. Stilborg, Temper for the sake of coherence: analyses of bone-and chaff-tempered ceramics from Iron Age Scandinavia, Eur. J. Archaeol. 4 (2001) 398–404.
[30] T.K. Perttula, Trubitt M. Beth, J.S. Girard, The use of shell-tempered pottery in the caddo area of the southeastern United States, SE, Near E. Archaeol. 30 (2011) 242–267.
[31] K.Yu Kiryushin, YuF. Kiryushin, I.G. Glushkov, The use of animal hair in ceramic manufacturing at the tytkesken-2 neolithic site, western siberia, Archaeol. Ethnol. Anthropol. Eurasia 40 (Issue 4) (2012), https://doi.org/10.1016/j.aeae.2013.04.005, 41–50.
[32] B. van Doosselaere, C. Delhon, E. Hayes, Looking through voids: a microanalysis of organic-derived porosity and bioclasts in archaeological ceramics from Koumbi Saleh (Mauritania, fifth/sixth–seventeenth century AD), Archaeol. Anthropol. Sci. 6 (2014) 373–396.
[33] V. Duckman, T. Kopar, Sawdust and paper-making sludge as pore-forming agents for lightweight clay bricks source, Ind. Ceram. 21 (2) (2001) 81–86.
[34] M. Sütçü, S. Akkurt, The use of recycled paper processing residues in making porous brick with reduced thermal conductivity, Ceram. Int. 35 (2009) 2625–2631.
[35] B. Ahmad, V. Yadav, A. Yadav, M.U. Rahman, W.Z. Yuan, Z. Li, X. Wang, Integrated biorefinery approach to valorize winery waste: a review from waste to energy perspectives, Sci. Total Environ. 719 (2020), 137315.
[36] T. Atatoprak, M.M. Amorim, T. Ribeiro, M. Pintado, A.R. Madureira, Grape stalk valorization for fermentation purposes, Food Chem.: Mol. Sci. 4 (2022), 100063, https://doi.org/10.1016/j.fochms.2021.100067.
[37] TOPAS Version 4.1, Bruker AXS, Karlsruhe, Germany, 2007.
[38] C. Coletti, G. Cultrone, L. Maritan, C. Mazzoli, Combined multi-analytical approach for study of pore system in bricks: how much porosity is there? Mater. Char. 121 (2016) 82–92, https://doi.org/10.1016/j.matchar.2016.09.024.
[39] UNI EN 13755, Natural Stone Test Methods - Determination of Water Absorption at Atmospheric Pressure, CNR-ICR, Rome, 2008.
[40] UNI EN 1925, Natural Stone Test Methods - Determination of Water Absorption Coefficient by Capillarity, CNR-ICR, Rome, 2000.
[41] C. Coletti, A. Borghi, R. Cossio, M.C. Dalconi, G. Dalla Santa, L. Peruzzo, R. Sassi, A. Vettorello, A. Galgaro, A multi-scale methods comparison to provide granitoid rocks thermal conductivity, Construct. Build. Mater. 304 (2021), 124612, https://doi.org/10.1016/j.jas.2021.105358.
[42] A. Hein, N.S. Müller, P.M. Day, V. Kilikoglou, Thermal conductivity of archaeological ceramics: the effect of inclusions, porosity and firing temperature, Thermochim. Acta 480 (2008) 35–42.
[43] I. Allegretta, G. Eramo, D. Pinto, A. Hein, The effect of mineralogy, microstructure and firing temperature on the effective thermal conductivity of traditional hot processing ceramics, Appl. Clay Sci. 135 (2017) 260–270.
[44] UNI EN 12371, Natural Stone Test Methods - Determination of Frost Resistance, CNR-ICR, Rome, 2010.
[45] UNI EN 12370, Natural Stone Test Methods - Determination of Resistance to Salt Crystallisation, CNR-ICR, Rome, 2001.
[46] L.N. Warr, IMA–CNMNC approved mineral symbols, Mineral. Mag. 85 (2021) 291–320, https://doi.org/10.1180/mgm.2021.43.
[47] G. Cultrone, E. Sebastián, M.J. de la Torre, Mineralogical and physical behaviours of solid bricks with additives, Construct. Build. Mater. 19 (2005) 39–48.
[48] L. Maritan, L. Nodari, C. Mazzoli, A. Milano, U. Russo, Influence of firing conditions on ceramic products: experimental study on clay rich in organic matter, Appl. Clay Sci. 31 (1–2) (2006) 1–15.
[49] C. Coletti, G. Cultrone, L. Maritan, C. Mazzoli, How to face the new industrial challenge of compatible, sustainable brick production: study of various types of commercially available bricks, Appl. Clay Sci. 124–125 (2016) 219–226, https://doi.org/10.1016/j.clay.2016.02.014.
[50] G. Cultrone, C. Rodriguez-Navarro, E. Sebastián, O. Cazalla, M.J. de la Torre, Carbonate and silicate phase reactions during ceramic firing, Eur. J. Mineral 13 (2001) 621–634.
[51] C. Coletti, L.P. Cesareo, J. Nava, L. Germinario, L. Maritan, M. Massironi, C. Mazzoli, Deterioration effects on bricks masonry in the Venice lagoon cultural heritage. Study of the main façade of the Santa Maria dei Servi Church (14th century), Heritage 6 (2) (2023) 1277–1292, https://doi.org/10.3390/heritage6020070.
[52] C. Rodriguez-Navarro, Técnicas de análisis del sistema poroso de un material pétreo ornamental, in: Cuadernos Técnicos n. 2: "Técnicas de diagnóstico aplicadas a la conservación de los materiales de construcción en los edificios históricos", Junta de Andalucía, Consejería de Cultura, 1996, pp. 51–65.
[53] S. Salvini, C. Coletti, L. Maritan, M. Massironi, A. Pieropan, R. Spiess, C. Mazzoli, Petrographic characterization and durability of carbonate stones used in UNESCO World Heritage Sites in northeastern Italy, Environ. Earth Sci. 82 (2023) 49, https://doi.org/10.1007/s12665-022-10732-y.